Calculation of RF sheath properties from surface wave-fields: a post-processing method

J.R. Myra

Lodestar Research Corporation, 2400 Central Avenue, Boulder, Colorado 80301, USA

and

H. Kohno

Department of Mechanical Information Science and Technology,
Kyushu Institute of Technology,680-4 Kawazu, Iizuka, Fukuoka 820-8502, Japan

April 2019

submitted to
Plasma Physics and Controlled Fusion

ORNL/4000158507-3; DOE-ER/54392-94 LRC-19-180

LODESTAR RESEARCH CORPORATION
2400 Central Avenue
Boulder, Colorado 80301

Calculation of RF sheath properties from surface wave-fields: a post-processing method

J R Myra[1] and H Kohno[2]

[1] *Lodestar Research Corporation, Boulder, CO 80301, USA*
[2] *Kyushu Institute of Technology, Iizuka, Fukuoka, 820-8502, Japan*

Abstract

In ion cyclotron range of frequency (ICRF) experiments in fusion research devices, radio frequency (RF) sheaths form where plasma, strong RF wave fields and material surfaces coexist. These RF sheaths affect plasma material interactions such as sputtering and localized power deposition, as well as the global RF wave fields themselves. RF sheaths may be modeled by employing a sheath boundary condition (BC) in place of the more customary conducting wall BC; however, there are still many legacy ICRF computer codes that do not implement the sheath BC. In this paper we present a method for post-processing results obtained with the conducting wall BC. The post-processing method produces results that are equivalent to those that would have been obtained with the RF sheath BC, under certain assumptions. The post-processing method is also useful for verification of sheath BC implementations and as a guide to interpretation and understanding of the role of RF sheaths and their interactions with the waves that drive them.

Keywords: radio frequency, ICRF, sheath, tokamak

1. Introduction

Ion cyclotron range of frequency (ICRF) waves are commonly used for heating and current drive in present day fusion research devices. Because of their flexibility and relatively low cost, ICRF systems are expected to play an increasing role in fusion-relevant plasmas for these applications and potentially others as well [1]. Compared with other auxiliary heating and current drive methods, the engineering challenges of ICRF systems are relatively minimal; however, a significant physics challenge remains: understanding and mitigating edge plasma interactions that are frequently observed in high power ICRF experiments [2-12].

It is believed that ICRF specific edge plasma interactions are often associated with the development of radio frequency (RF) sheaths [13-15]. RF sheaths form where plasma, strong RF wave fields and material surfaces coexist. They result in enhanced plasma potentials relative to the wall, and therefore they increase the energy at which ions strike the surface and sputter impurities [4,8]. RF sheaths can also lead to enhanced plasma convection [3,16,17] and surface power deposition [18-20], which may be localized and cause material damage or enhanced erosion. For all of these reasons, RF sheaths have been the subject of many theoretical and modeling studies [13-16, 19-30].

RF sheaths exist on the scale of a few to a few tens of Debye lengths, much smaller than typical RF wavelengths or the global scale of fusion research devices. Consequently, it is possible to model an RF sheath on the global scale by means of a boundary condition (BC), specifically a sheath BC on the solution for the RF waves [19, 31,32]. In this paper, we adopt the sheath BC formulation of Refs. [19, 33] which provides an effective surface impedance seen by the RF waves, as a function of plasma, geometric and RF parameters. The sheath BC also allows calculation of the "rectified" sheath voltage, and total instantaneous sheath voltage available for ion acceleration and sputtering, as well as the RF sheath power dissipation which appears as a heat load on the surface.

The goal of this paper is to enable RF sheath calculations from RF wave-fields that were obtained under the conducting wall (CW) BC. The original motivation came from the fact that many legacy RF codes still use the CW-BC. It would be useful to have a means of obtaining some information, even if approximate, about sheaths from these codes. Secondly, as modern codes begin to implement the sheath BC, it will be useful to have a method of verification. The sheath post-processing method described here should

address that need. Finally, the post-processing method can be useful for interpretation, analysis and as a guide to intuition concerning the role of RF sheaths in a given situation.

Details of the post-processing method and its testing constitute the bulk of this paper. At a high level, we can describe the basic idea as follows. An observer located at the bounding surface of the plasma sees incoming and outgoing waves as well as certain field quantities on the surface itself. The relationship of the outgoing waves to the incoming waves depends on the BC. If the incoming waves are not dependent on the outgoing waves (an exception would be that of a resonant cavity) then it should be possible, given sufficient information collected at the surface under one type of BC, to transform that solution to another solution under a different type of BC. All of the required calculations would be local to the surface, and they would assume that under the change of BC, the incoming waves would remain unchanged. We illustrate this method specifically for the transformation of CW-BCs to sheath BCs, although the method itself is really quite general. In order for the post-processing calculations to be semi-analytical, we assume that the plasma and geometrical parameters are constant on and near the surface. This paper generalizes a previous exploratory attempt along these lines, presented in Ref. [34]. That paper was restricted to slow wave polarizations and perpendicular incidence of the magnetic field lines on the surface (hence effectively unmagnetized sheaths). Here we consider a general formation retaining both fast and slow wave polarizations with application to oblique angle sheaths.

The plan of our paper is as follows. In Sec. 2 we describe in detail the basic equations and method. This includes a brief review of the sheath BC, the equations for the incoming and outgoing wave fields near the surface, the method of solution and a simple analytic example. Sec. 3 provides numerical verification tests for one dimensional (1D) and two dimensional (2D) examples. Results verify both the post-processing method and the rfSOL code [20,35] which was used for comparison. A summary and our conclusions follow in Sec. 4. Some technical details of the solution of Maxwell's equations and of the sheath BC are given in the appendices.

2. Basic equations and method

2.1 Sheath boundary condition

A sheath BC was derived from a Debye-scale model in Ref. [19] and later the results of that model for voltage rectification and RF sheath impedance were parametrized in Ref. [33]. A description of the physics contained in this model is beyond

the scope of the present paper. Here, we shall simply quote the mathematical form of the sheath BC and regard the sheath impedance parameter z_{sh} as a known input for given plasma, geometrical and RF parameters. Specifically, examples in this paper use the parametrization [33] $\hat{z}(\hat{\omega},\hat{\Omega},b_n,\xi)$ where $\hat{\omega} = \omega/\omega_{pi}$, $\hat{\Omega} = \Omega_i/\omega_{pi}$, $b_n = \mathbf{s}\cdot\mathbf{b}$ and $\xi = e|V_{sh}|/T_e$. Here the dimensionless quantity $\hat{z}$ is related to the sheath impedance parameters z_{sh} in SI units by $z_{sh} = \hat{z}\lambda_d/(\varepsilon_0\omega_{pi})$. Also, ω is the applied RF frequency, ω_{pi} is the ion plasma frequency, Ω_i is the ion cyclotron frequency, **s** is the unit normal to the surface pointing into the plasma (**n** is reserved for the RF index of refraction), $\mathbf{b} = \mathbf{B}_0/B_0$ is the direction of the equilibrium magnetic field, T_e is the electron temperature, and $|V_{sh}|$ is the (zero-to-peak) amplitude of the RF wave at the sheath interface. The post-processing method described in the following does not depend on this particular parametrization of the BC: any expression for z_{sh} could be used.

The sheath BC may be written as

$$\mathbf{E}_t = \nabla_t (J_n z_{sh}) \tag{1}$$

where **E** is the RF electric field and J_n is the total RF current density (particle plus displacement current) on the plasma side of the sheath, and the subscripts t and n denote the surface tangential and normal components, respectively. Note that when $z_{sh} = 0$, the sheath BC reduces to the usual CW-BC, i.e. the tangential electric field vanishes on the boundary. It is sometimes convenient to employ the total displacement vector $\mathbf{D} = \varepsilon_0 \overline{\overline{\varepsilon}}\cdot\mathbf{E}$ which is related to the total current density by

$$\omega\mathbf{D} = i\mathbf{J} \tag{2}$$

where $\overline{\overline{\varepsilon}}$ is the relative permittivity tensor and we adopt the convention that the RF waves vary like $\exp(i\mathbf{k}\cdot\mathbf{x}-i\omega t)$. For notational brevity, this phase factor will be implicit in most of the subsequent discussion.

2.2 Equations for the waves

We begin with a 1D geometry, illustrated in Fig. 1, in which the waves propagate in the x direction and encounter a planar surface, in general rotated through an angle φ along the z axis. At the surface, we regard the incoming waves as known, with given values of tangential wavevector $\mathbf{k}_t$ on the surface. (A superposition of $\mathbf{k}_t$ components obtained by Fourier analysis is also permitted.) The RF waves in the source-free homogeneous plasma volume obey the Maxwell equation

$$\mathbf{n}\times(\mathbf{n}\times\mathbf{E}) + \overline{\overline{\varepsilon}}\cdot\mathbf{E} = 0 \tag{3}$$

where $\mathbf{n} = \mathbf{k}c/\omega$ and ω are also specified.

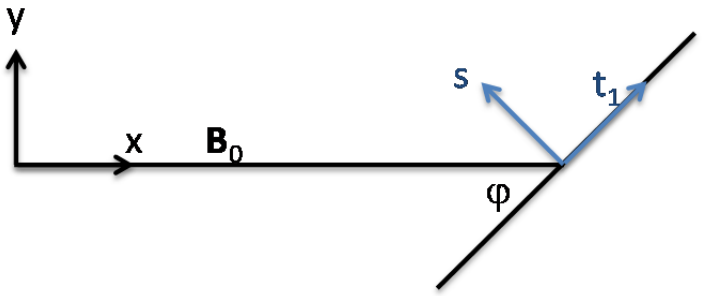

Fig. 1 Geometry for the solution of Maxwell's equations. The unit normal pointing from the surface into the plasma is **s**, and $\mathbf{t}_1$ is the unit vector along the surface in the x-y plane. The equilibrium magnetic field direction is $\mathbf{b} = \mathbf{e}_x$.

The unknowns in Eq. (3) are the generalized eigenvalues k_n (or equivalently n_n) and the associated eigenvectors **E**. It is shown in Appendix A that Eq. (3) may be rewritten in the form of a generalized eigenvalue problem for k_n by splitting it up into the two original constituent Maxwell equations for the RF fields **E** and **B**. The solution provides four normal modes, $k_n^{(m)}$ and their associated electric field polarization unit vectors $\mathbf{e}^{(m)}$, m = 1, … 4. The four modes are the fast and slow waves, each with two directions of propagation (or evanescence). Thus the total electric field is expressed as

$$\mathbf{E} = \sum_m E^{(m)} \mathbf{e}^{(m)} \tag{4}$$

where the complex amplitudes $E^{(m)}$ are to be determined. The general set of equations coupling $E^{(m)}$ and the surface field quantities J_n and $\mathbf{B}_t$ are

$$-i\omega\varepsilon_0 \, \mathbf{s} \cdot \overline{\overline{\varepsilon}} \cdot \left(\sum_m E^{(m)} \mathbf{e}^{(m)} \right) = J_n \tag{5}$$

$$\left(\sum_m E^{(m)} \mathbf{e}^{(m)} \right) \cdot \mathbf{e}_t = ik_t z_{sh} J_n \tag{6}$$

$$\left(\sum_m E^{(m)} \mathbf{e}^{(m)} \right) \cdot \mathbf{e}_z = ik_z z_{sh} J_n \tag{7}$$

$$-\frac{1}{\omega} \sum_m E^{(m)} k_n^{(m)} \, \mathbf{s} \cdot (\mathbf{k}^{(m)} \times \mathbf{e}^{(m)}) = \mathbf{k}_t \cdot \mathbf{B}_t \tag{8}$$

Recall that **s** is the unit normal pointing from the surface into the plasma so that $J_n = \mathbf{J} \cdot \mathbf{s}$. Equation (8) is obtained from $\mathbf{k} \times \mathbf{E} = \omega \mathbf{B}$ by dotting with **s**, multiplying by k_n and using $k_n B_n = -\mathbf{k}_t \cdot \mathbf{B}_t$ for each of the $\mathbf{k}^{(m)}$, $\mathbf{E}^{(m)}$ and $\mathbf{B}^{(m)}$ modes under the summation. This

manipulation is employed for numerical accuracy reasons but also possess an aesthetically pleasing symmetry: $J_n \propto \mathbf{s}\cdot\mathbf{k}_t\times\mathbf{B}_t$ is one "source" term, while the complementary quantity $\mathbf{k}_t\cdot\mathbf{B}_t$ is the other.

Here for pedagogical simplicity we have written the equations in Fourier component form for the case of constant z_{sh}. An important generalization will be discussed subsequently.

The equation set, Eqs. (4) – (7), may be used to solve for any four of the six quantities $E^{(m)}$, m = 1, ... 4, J_n and $\mathbf{k}_t\cdot\mathbf{B}_t$ given any two of them. Two different sets of given quantities and unknowns will be employed for the complete post-processing procedure.

2.3 Solution method

The post-processing procedure for transforming a CW solution into a sheath BC solution is as follows.

(i) First, one obtains, from the CW solution, the quantities $J_{n,cw}$ and $\mathbf{k}\cdot\mathbf{B}_{t,cw}$ on the surface.

(ii) Given these quantities, and setting $z_{sh} = 0$, corresponding to the CW solution from which they came, Eqs. (4) – (7) are solved for $E_{cw}^{(m)}$, m = 1, ... 4, thus determining the incoming and outgoing fast and slow waves incident on the surface. For the sake of discussion, we will regard m = 1, 2 as the incoming waves, and m = 3,4 as the outgoing waves. For propagating modes, the incoming or outgoing status is determined by the sign of the group velocity. For evanescent modes, it is determined by the direction of exponential decay.

(iii) Having determined the amplitude coefficients of the incoming waves, which are now to be held fixed, the final step is to regard $E_{cw}^{(1)}$ and $E_{cw}^{(2)}$ as source terms, and solve for the outgoing waves, the surface current and the tangential magnetic field using the sheath BC. This step therefore employs the desired value of z_{sh}, and the solution yields quantities we label as $E_{sh}^{(3)}$, $E_{sh}^{(4)}$, $J_{n,sh}$ and $\mathbf{k}\cdot\mathbf{B}_{t,sh}$.

The procedure is conceptually straightforward, but is complicated by two issues. The first is that z_{sh}, as given in Ref. [33] is a nonlinear function of the RF amplitude on the surface. This means that step (iii) must be iterated, with z_{sh} updated on each iteration

until convergence is achieved. Namely, at each iteration the RF sheath voltage is determined from

$$V_{sh} = -J_n z_{sh} \tag{9}$$

and then $\xi = |eV_{sh}/T_e|$ is used to determine $z_{sh} = z_{sh}(\xi)$ for the next iteration. For all the examples that have been tried in preparing this paper, a simple fixed point iteration converges well.

The second complicating issue is also related to the nonlinearity. Because the RF amplitude in general varies along the surface, z_{sh} is not a constant spatially in a given iteration step. This couples the various $\mathbf{k}_t$ Fourier modes on the surface and means that in practice, Eqs. (4) – (7) are in fact replaced by more complicated matrix equations which are described in Appendix B. These equations still use the same solution of Maxwell's equations in Fourier space for each of the component Fourier modes, but the modes are coupled together.

Once a converged solution is obtained, the final RF sheath voltage is given from Eq. (9). From it, the rectified DC voltage may be calculated from a simple fit [33] and also using $J_{n,sh}$ the RF surface power dissipation per unit area may be calculated from

$$P = -\frac{1}{4} J_n V_{sh}^* + cc = \frac{1}{2} |J_n|^2 \, \mathrm{Re}(z_{sh}) \tag{10}$$

For a flat wall with constant plasma and magnetic field parameters, the preceding method is exact (assuming that the modified outgoing waves do not affect the incoming waves), as demonstrated in Sec. 3.1. In this case the procedure can be used to verify an implementation of the sheath BC in an RF code.

For a shaped wall, or when there is variation of the plasma or magnetic field parameters, the procedure may be invoked in a local sense at each point on the surface, and will be valid when the local approximation for the RF waves is valid. A typical sufficient condition is $k_t L >> 1$ where L is the scale length of variation along the surface. Later, we will also discuss another limit in which the post-processing method is exact, even for a shaped wall.

2.4 An analytic example

A simple analytical example, discussed in Ref. [34], is useful for illustrating both the procedure and the power of the method. This example is given for the electrostatic limit in the case of a flat wall with normal vector $\mathbf{s} = -\mathbf{e}_x$ corresponding to $\varphi = \pi/2$ in Fig.

1 and background magnetic field $\mathbf{B}_0 = B_0\,\mathbf{e}_x$. The general solution for an RF wave in the electrostatic limit consists of just the incoming slow wave (m = 1) and the outgoing slow wave (m = 3).

$$\mathbf{E} = -i\mathbf{k}^{(1)}\Phi^{(1)}e^{ik_x^{(1)}x} - i\mathbf{k}^{(3)}\Phi^{(3)}e^{ik_x^{(3)}x} \tag{11}$$

where $\Phi^{(1)}$ and $\Phi^{(3)}$ are the amplitudes of the electrostatic potential. The total potential at the wall, taken to be at x = 0, is $\Phi = \Phi^{(1)} + \Phi^{(3)}$. For the CW solution, which is presumed to be known, this must be zero hence $\Phi_{cw}^{(3)} = -\Phi_{cw}^{(1)}$. Furthermore, in this geometry the incoming and outgoing wavevectors will have equal and opposite normal components, $k_n^{(3)} = -k_n^{(1)}$. The resulting normal component of the electric field at the wall for the CW case is therefore

$$E_n, cw \equiv E_{n,cw}^{(1)} + E_{n,cw}^{(3)} = -2ik_n^{(1)}\Phi_{cw}^{(1)} \tag{12}$$

The normal current at the surface J_n for the CW case is related to this electric field by Eq. (5). This enables the determination of the incoming wave amplitude $\Phi_{cw}^{(1)}$ in terms of $J_{n,cw}$ completing step (ii) of the post-processing procedure.

$$\Phi_{cw}^{(1)} = -\frac{J_{n,cw}}{2\omega\varepsilon_0\varepsilon_{||}k_n^{(1)}} \tag{13}$$

Note that $k_n^{(1)}$ is determined by the slow wave dispersion relation given k_y and k_z on the surface,

$$k_\perp^2\varepsilon_\perp + k_{||}^2\varepsilon_{||} = 0 \tag{14}$$

which plays the role of the Maxwell solution in the general case.

Step (iii) is to use $\Phi_{cw}^{(1)}$ as the source term for a new solution which retains the sheath BC, in particular finite z_{sh}. The relevant equations are Eqs. (5) and (6) or (7). Eq. (8) is not relevant for electrostatics, and Eqs. (6) and (7) are just the tangential gradient of Eq. (9) where $V_{sh} = \Phi^{(1)} + \Phi^{(3)}$. Holding $\Phi_{cw}^{(1)}$ fixed and regarding J_n and $\Phi^{(3)}$ as the new unknowns, the equations to be solved therefore are,

$$-\omega\varepsilon_0\,\varepsilon_{||}k_n^{(1)}(\Phi_{cw}^{(1)} - \Phi^{(3)}) = J_n \tag{15}$$

$$\Phi_{cw}^{(1)} + \Phi^{(3)} = -J_n z_{sh} \tag{16}$$

where $k_n^{(3)} = -k_n^{(1)}$ has again been used in Eq. (15). Solving for J_n and $\Phi^{(3)}$ and then forming V_{sh} one obtains

$$J_{n,sh} = \frac{J_{n,cw}}{1-\rho} \tag{17}$$

$$\Phi_{sh}^{(3)} = -\frac{J_{n,cw}\, z_{sh}(1+\rho)}{2\rho(1-\rho)} \tag{18}$$

$$V_{sh} = \Phi_{cw}^{(1)} + \Phi^{(3)} = -\frac{J_{n,cw} z_{sh}}{1-\rho} \tag{19}$$

where

$$\rho = -\omega\varepsilon_0\, \varepsilon_{||} k_n^{(1)} z_{sh} \tag{20}$$

This expresses the desired sheath quantities in terms of the input $J_{n,cw}$ and completes the post-processing method in this simple electrostatic model.

The point of this analytical electrostatic exercise is to illustrate how the process works with a concrete example, and to point out several features of the solution which also apply to the numerical 2D electromagnetic case. These features are evident from the result for V_{sh} which is usually the main output of interest. The first point is that Eq. (19) is a nonlinear equation for V_{sh} since $\rho \propto z_{sh}$ is itself a function of $|V_{sh}|$. The second point is evident from the form of the denominator which displays a resonance at $\rho = 1$ This is the sheath-plasma wave resonance [20,36,37]. Related to this point is the fact that Eq. (19) illustrates the different regimes of the wave interaction with the sheath [38]. For $|\rho| << 1$ the sheath is in the conducting limit where the sheath voltage is small, while in the opposite limit $|\rho| >> 1$ the sheath is in the quasi-insulating limit. Note that in the conducting limit $V_{sh} = -J_{n,cw}\, z_{sh}$; in this case although the equation for V_{sh} is still nonlinear, it does not involve any additional solution of the Maxwell equations: the sheath voltage is available directly and exactly from the CW solution and the knowledge of z_{sh}. This is one of a few cases in which the post-processing method is exact.

For future reference, the form of ρ, when generalized to arbitrary magnetic field angles with the surface, is given in the electrostatic limit as [38]

$$\rho = \omega\varepsilon_0 \mathbf{s} \cdot \bar{\bar{\varepsilon}} \cdot \mathbf{k}_n^{(3)} z_{sh} \tag{21}$$

When **b** and **n** are collinear, $k_n^{(3)} = -k_n^{(1)}$ but this is not generally true for magnetic fields that are oblique to the surface.

3. Verification tests

In this section several verification tests of the post-processing method are presented. Verification is obtained by comparing the results of the post-processing analysis with results obtained from the rfSOL code [35]. The rfSOL code has within it a complete implementation of the sheath BC. In situations for which the post-processing method is exact, agreement with rfSOL may be taken as evidence for verification of both the post-processing method and rfSOL itself. In situations for which the post-processing method is approximate, verification tests provide information about the expected accuracy of post-processing and reveal the relevant dimensionless parameters controlling that accuracy.

3.1 Test #1: verification with a flat wall

Verification test #1 is for a flat wall case. It uses the coupled Fourier mode approach described in Appendix B and therefore should provide an exact solution of the post-processing problem. The 2D geometry for the test is shown in Fig. 2. In the third (z) direction the equilibrium is ignorable and a plane wave is assumed. Thus all quantities in this analysis are implicitly proportional to $\exp(ik_z z - i\omega t)$.

The plasma and RF parameters for this test are: $n_e = 6.0\times10^{17}$ m^{-3}, Z = 1, A = 2 (deuterium), T_e = 10 eV, (B_x, B_y, B_z) = (0.5, 1.5, 4.) T, k_z = 10.8 /m and $\omega/(2\pi)$ = 80 MHz. The maximum in y of the antenna current for this case is K_{max} = 60 A/m. Thus this case employs oblique angle sheaths in slab geometry with constant plasma parameters. Although rfSOL and the post-processing analysis retain both fast and slow waves, in this test the antenna dominantly launches an evanescent slow wave. The "incoming" branch (i.e. the one that decays as it approaches the wall) interacts with the right wall BC and reflects onto the "outgoing" branch which decays away from the wall.

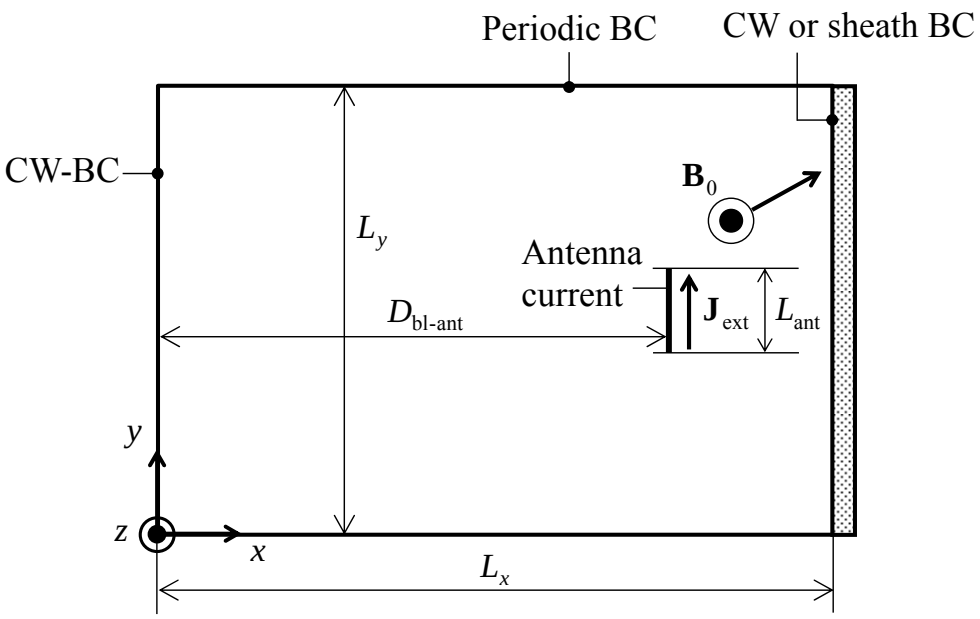

Fig. 2 Geometry for verification test #1. The antenna is located at x = 0.47 m and the wall is at L_x = 0.5 m. The antenna height in y is L_{ant} = 0.05 m. The domain is periodic in the y direction with box size L_y = 0.4 m. See Ref. [35] for additional information about rfSOL.

The steps for this test are as follows: (i) rfSOL is run with the CW-BC at x = L_x; (ii) the data for $J_{n,cw}$ and $\mathbf{k}\cdot\mathbf{B}_{t,cw}$ are passed to the post-processing scripts; (iii) the post-processing analysis is run and $V_{sh,pp}$ and $J_{n,sh,pp}$ are calculated; (iv) an independent run of rfSOL is done with the sheath BC to calculate $V_{sh,rfSOL}$ and $J_{n,sh,\,rfSOL}$; (v) the post-processing results $V_{sh,pp}$ and $J_{n,sh,pp}$ are compared with the rfSOL results $V_{sh,rfSOL}$ and $J_{n,sh,,rfSOL}$.

The result for the conducting wall solution for $D_{n,cw} = i\, J_{n,cw}/\omega$ along the sheath surface as obtained from step (ii) is shown in Fig. 3. The evanescent slow wave launched from the antenna impacts the wall above the midplane y = 0.2 m, since the fields approximately follow obliquely tilted field lines. In addition to $J_{n,cw}$ the profile of $\mathbf{k}\cdot\mathbf{B}_{t,cw}$ is also passed to the post-processor ; however, $\mathbf{k}\cdot\mathbf{B}_{t,cw}$ does not significantly affect the result and is not shown.

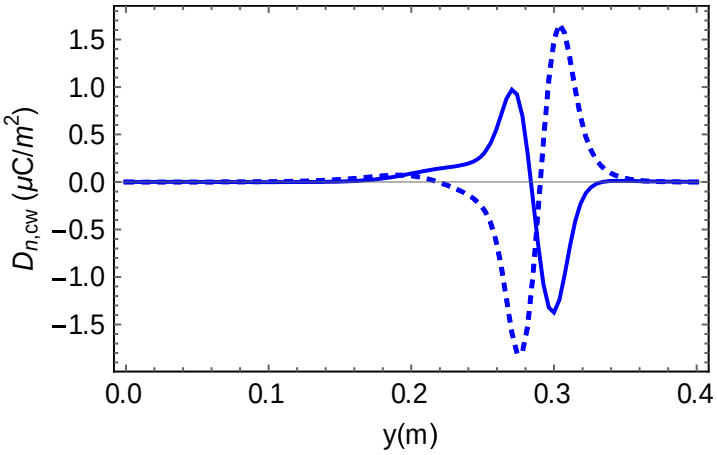

Fig. 3 The CW solution for D_n along the sheath surface from rfSOL for test #1. Real and imaginary parts of D_n are indicated in solid and dashed lines respectively.

The next step, step (iii), is the post-processing itself, as described in Sec. 2.3. In Fig. 4 the convergence of the solution under the nonlinear iteration is shown. The figure represents 12 separate linear post-processing sub-calculations to obtain the final nonlinearly converged result. In this case the initial condition for the first iteration was $V_{sh} = 0$ and a simple fixed point (Picard) iteration was employed. Convergence to the final result is robust and sufficiently rapid. Additional runs (not shown) with an initial condition of very large V_{sh} were also found to converge to the same result at a similar rate and in a similar number of iterations.

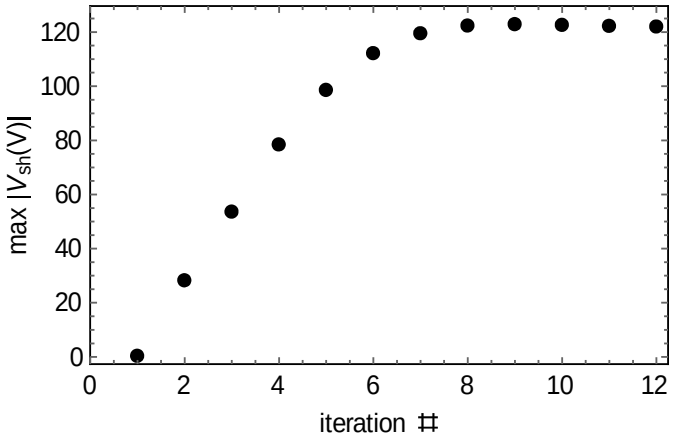

Fig. 4 Convergence of the nonlinear iteration for test #1 with the initial condition $V_{sh} = 0$. The plot shows the maximum value of $|V_{sh}(y)|$ for each iteration step.

Step (iv) is to generate an independent result using the sheath BC in the rfSOL code, and finally step (v) is to compare the rfSOL result from step (iv) with the sheath post-processing method. That comparison is shown in Fig. 5.

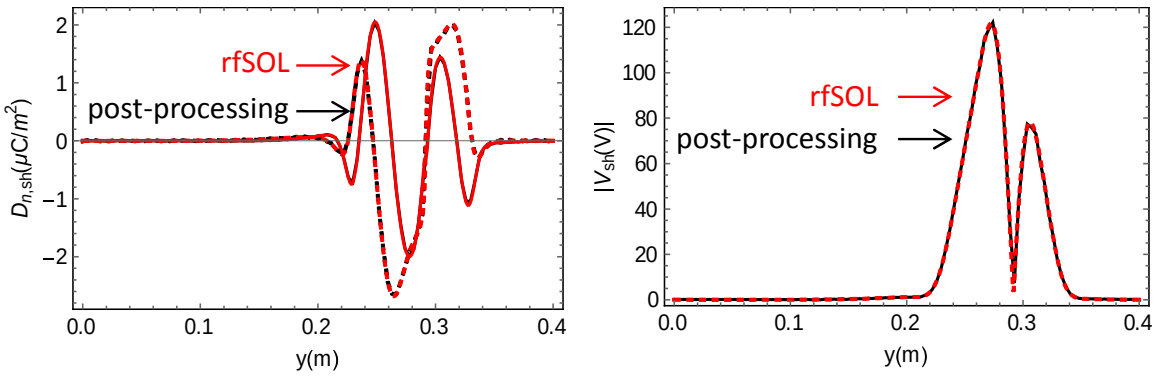

Fig. 5 Comparison of the post-processing result (black) with the rfSOL result (red) for test #1: left panel $D_{n,sh}$; right panel $|V_{sh}|$. Real and imaginary parts of $D_{n,sh}$ are indicated in solid and dashed lines respectively.

From Fig. 5 it can be seen that the agreement is excellent as it should be: this is one of the cases for which the post-processing method is exact, in principle. Comparing the conducting wall and sheath solutions for D_n in Figs. 3 and 5 it can be seen that the sheath BC has changed the structure of D_n and hence J_n significantly. This implies that for the parameters of this test, the sheath is far from the conducting limit.

3.2 Test #2: verification with a shaped wall

The rfSOL geometry for test #2, illustrated in Fig. 6, is similar to test #1, but with a shaped wall. The shape is obtained by deforming the wall with a Gaussian bump given by $h(y) = h_b \exp[-(y-y_0)^2/w_b^2]$. Because the wall is shaped, it is no longer feasible to use the post-processing Fourier method to implement the sheath BC. Instead for this case the approximate local method is used. This means that it is necessary to specify a value for k_y. The dominant k_y launched by the antenna is approximately $k_y = \pi/L_{ant}$ where L_{ant} = 0.40 m is the length of the antenna in the y direction. The parameters for this case are: $n_e = 1.0\times10^{18}$ m^{-3}, Z = 1, A = 2 (deuterium), T_e = 15 eV, (B_x, B_y, B_z) = (4.0, 0.0, 0.0) T, k_y = 15.7 /m, k_z= 160. /m, $\omega/(2\pi)$ = 80 MHz and K_{max} = 9 kA/m. The bump shape parameters are $y_0 = L_y/2$, h_b = 0.4 m and w_b = 0.1 m

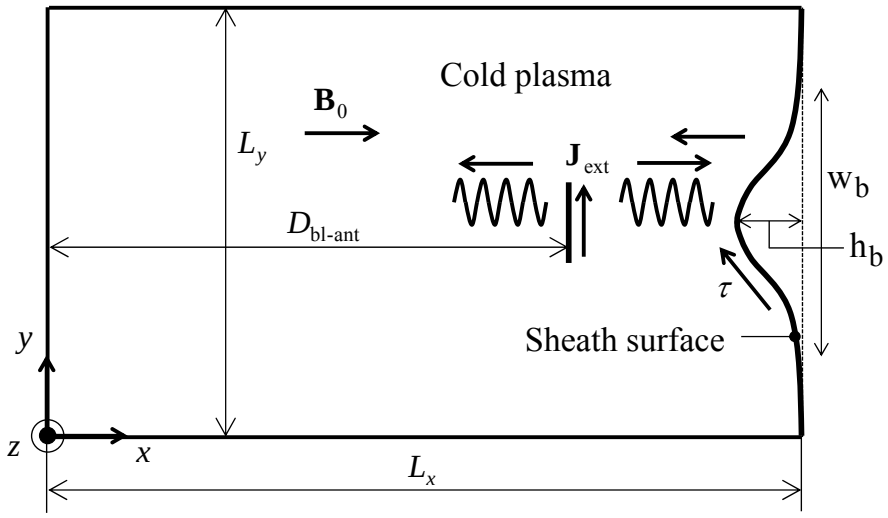

Fig. 6 Geometry for verification test #2. Except for the shaping of the right wall, the rfSOL setup is similar to that for test #1 but with different parameters. The antenna is located at x = 2.26 m and the wall is at L_x = 3.0 m. The antenna height in y is L_{ant} = 0.4 m. The domain is periodic in the y direction with box size L_y = 0.8 m. The bump parameters are h_b = 0.4 m and w_b = 0.1 m. See Ref. [35] for additional information about rfSOL.

Other than the use of the local method, the steps are the same as in test #1. At each point along the sheath surface, the local angle of the magnetic field with respect to the surface is employed both for computing k_n in the solution of Maxwell's equations and in the argument of the sheath impedance. Results for the RF sheath voltage are shown in Fig. 7. It can be seen that in spite of the local approximation, the agreement of the post-processing method with rfSOL is excellent. The main reason for this is the large value of k_z = 160/m. Since the scale length of variation of the bump L is of order w_b = 0.1 m, $k_z L$ = 16 >> 1, so we expect local theory to be a good approximation. Furthermore because $k_y << k_z$, and both directions are perpendicular to B, the choice of k_y is not particularly critical.

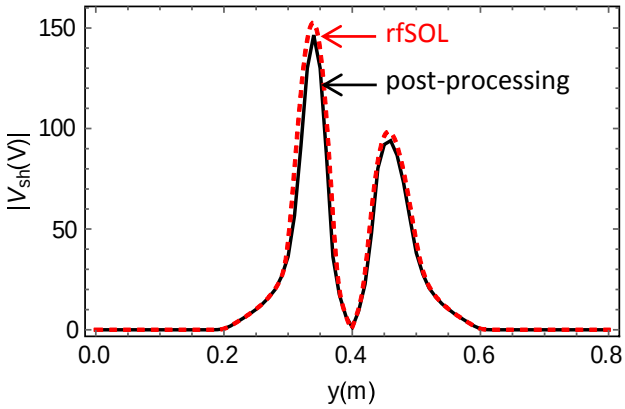

Fig. 7 Comparison of the RF sheath voltage post-processing (black) result with the rfSOL (red) result for test #2.

Thus, this case verifies the implementation of the local post-processing method, but does not provide much of a guide to its usefulness in more general cases. That question will be addressed in the next sub-section. First we demonstrate another feature of the post-processing method.

Because the inputs to the post-processing method are $J_{n,cw}$ and $\mathbf{k}\cdot\mathbf{B}_{t,cw}$ from the conducting wall solution, and that solution is strictly linear, $J_{n,cw}$ and $\mathbf{k}\cdot\mathbf{B}_{t,cw}$ can be rescaled to different values of the antenna current K_{max} than were originally used. This means that the CW solution can be post-processed for a scan in K_{max} from a single CW case. Results for such a scan are shown in Fig. 8.

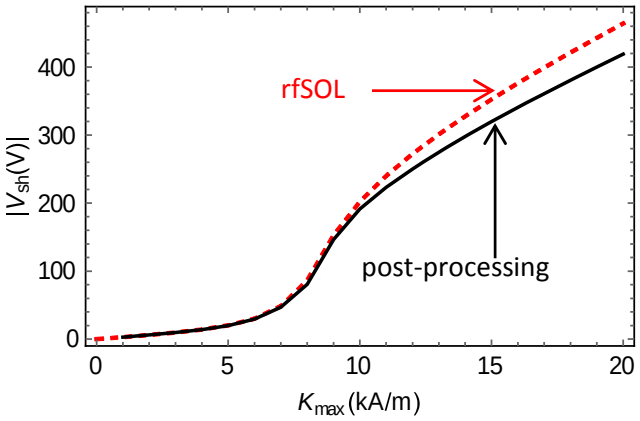

Fig. 8 Comparison of results for the maximum of $|V_{sh}|$ over y from rfSOL and the post-processing method using the parameters of test #2, except for K_{max} which is scanned. The base case for test #2, shown in Fig. 7, is for K_{max} = 9 kA/m,

Fig. 8 shows agreement for small values of K_{max}, with growing discrepancies as K_{max} is increased and $|V_{sh}|$ becomes large. The reason for this is that as the nonlinearity increases at high $|V_{sh}|$ the solution develops short scale-length structure near the peak values of $|V_{sh}|$ causing the accuracy of the local approximation to deteriorate. However, qualitative features present in the more accurate rfSOL result are still quite evident. In particular, the three regimes of the RF wave interaction with the sheath are present, For $K_{max} < 6$ kA/m the sheath is in a conducting and nearly linear regime. In this regime, as discussed above, V_{sh} is independent of the approximations of the local method, and the result comes directly from $J_{n,cw}$ in analogy to the electrostatic result shown in Eq. (19) for $|\rho| << 1$. For intermediate K_{max} in the range 6 kA/m < K_{max} < 11 kA/m, the interaction crosses a dissipative sheath-plasma wave resonance and $|V_{sh}|$ rises rapidly with K_{max}. In this case the z_{sh} term, i.e. ρ in the denominator of Eq. (19), is of order unity. Finally for $K_{max} > 11$ kA/m the RF wave-sheath interaction enters the quasi-insulating regime for which the ρ term in the denominator of Eq. (19) begins to exceed unity. A more detailed discussion of the sheath regimes and their interaction with RF waves is given in Refs. 35 and 38.

3.3 Test #3: limitations of the local method

Test #3 was constructed to be more challenging for the post-processing method, in order to demonstrate its limitations. Thus, we continue to use the shaped wall which requires the local approximation, but now we choose a smaller value of $k_z = 40$ /m to reduce k_z L and we choose a value of $K_{max} = 5.46$ kA/m that is just beyond the sheath-plasma wave resonance. Smaller values of k_z tend to reduce ρ according to Eq. (21), causing the sheath to enter the conducting limit. This would be contrary to the desired test. Choosing K_{max} too near the sheath plasma wave resonance would not provide a useful test case as results can be very sensitive in that region. On the other hand, for K_{max} well below the resonance, it is expected and verified that the post-processing and rfSOL results agree very well, since then the simplifications of the conducting sheath regime apply. Except for k_z and K_{max}, other parameters for test #3 are the same as in test #2.

Results are shown in Fig. 9. For this case the agreement is only qualitative, especially near the peak values of $|V_{sh}|$ in the range 0.4 m < y < 0.55 m. It is in this range that the local sheath parameters depart strongly from the conducting sheath limit. Outside of this range, where the sheath voltages are smaller, and the sheath is once again in the conducting limit, the local approximation is accurate. Although the post-processing method only gives a rough approximation to the rfSOL result, it correctly predicts the

location of the peak voltage, and the fact that the peak voltage is extremely *large*: either 870 V (post-processing) or 1230 V (rfSOL) would in practice be of significant concern for plasma material interactions.

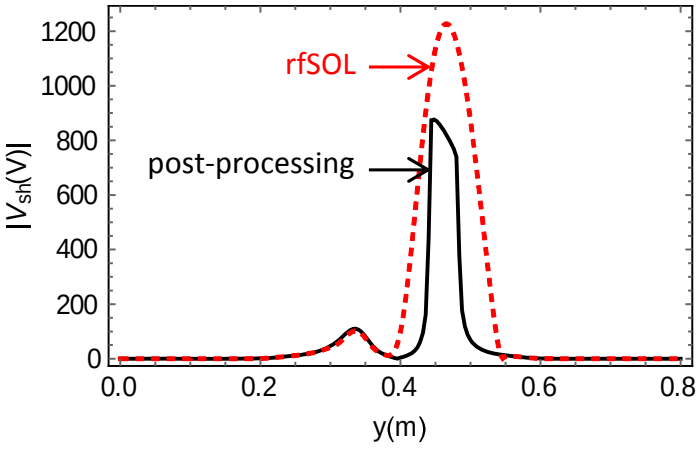

Fig. 9 Comparison of the post-processing result (black) with the rfSOL result (dashed red) for the RF sheath voltage in test #3.

4. Summary and conclusions

In this paper, we have presented a post-processing method for evaluation of RF sheath properties and RF sheath-wave interactions. The post-processing method accepts as input two scalar quantities from a simulation code that employs conducting wall boundary conditions: (i) the RF current normal to the conducting surface and (ii) the divergence of the RF magnetic field in the tangential plane of the surface. From these inputs the method produces, under some assumptions, results that would have been obtained had the original simulation been performed with an RF sheath boundary condition. In particular, an output of the method is the RF sheath voltage. Using methods explained in previous published works, [19,33] this enables a calculation of the "rectified" DC sheath potential for sputtering as well as a calculation of the RF sheath power dissipation which appears as a heat load on the surface.

The main assumption that makes the post-processing method possible is the assumption that the RF wave propagating *towards* the boundary remains unchanged by changing the boundary condition from that of a conducting wall to a sheath boundary condition. This condition is expected to hold in many cases, with a notable exception being that of a resonant cavity where the outgoing wave (propagating away from the

boundary) is reflected elsewhere in the system and mixes with or becomes the incoming wave on a later pass.

Additional assumptions of the method as implemented here are constant or at least slowly varying plasma parameters, magnetic field and unit surface normal along the sheath surface.

In this paper we have demonstrated how the post-processing method may be iterated to obtain RF field solutions that are self-consistent with the nonlinear sheath impedance boundary condition. For all the cases investigated, a simple fixed point iteration scheme converged well. Results were compared with solutions obtained from the rfSOL code, a full wave code with shaped wall capabilities that employs the self-consistent sheath BC with nonlinear iteration.

Two implementations of the post-processing method were demonstrated. The first one is exact and applies to a flat wall. In this case, the method is applied to each Fourier mode on the wall. Although the sheath nonlinearity induces spatial variation of the sheath impedance boundary condition, and this couples the Fourier modes, the problem reduces to that of a modestly large matrix equation which may be readily solved by standard numerical packages. The second implementation applies to a shaped wall or when plasma or magnetic field parameters vary along the surface. In this case a local approximation method is used which requires estimation of the tangential component of the wavevector $\mathbf{k}_t$ of the incoming waves. The local method is theoretically justified when $k_t L > 1$ where L is the scale length of variation along the surface.

We have seen from the examples presented that the post-processing method is exact or becomes exact in the limit of a small or large parameter. The situations leading to an exact result are as follows: (i) a flat surface with constant plasma and magnetic field parameters (for any values of ρ or k_z), (ii) a shaped surface with the sheath in the conducting limit, $|\rho| << 1$, or (iii) a gently shaped surface such that local theory is valid, $k_z L >> 1$. In all other cases, the post-processing method is approximate. An estimate of ρ based on electrostatic theory may be obtained from Eq. (21).

Although it is expected that a sheath boundary condition will eventually be implemented in most RF simulation codes intended for boundary plasma analysis, the post-processing method may provide a useful means of sheath modeling for some legacy RF codes. Furthermore, for codes which do implement the sheath BC, the method may be useful in speeding up nonlinear convergence by supplying an approximate solution as an initial guess. In simple geometries the post-processing method may be used as a tool to

verify correct implementation of the sheath boundary condition. Finally, the method and the examples shown here should help to improve understanding and intuition for the behavior of RF wave and sheath interactions.

Much future work remains to enable quantitative modeling of ICRF boundary plasma interactions. RF sheath potentials should be coupled to kinetic simulation codes to calculate ion distribution functions impacting the wall, and the resulting impurity sputtering fluxes, [39] and the migration of those fluxes throughout the plasma. The micro-scale (Debye-scale) theory of RF sheaths giving rise to the sheath impedance employed in the examples of this paper should be verified against experiments and generalized as necessary to improve its fidelity. RF specific sheath power dissipation on all surfaces of the device vessel should be calculated in realistic geometry. Complex workflows will be required for this program and are under development in the larger RF fusion community.

Acknowledgments

This material is based upon work supported by the U.S. Department of Energy Office of Science, Office of Fusion Energy Sciences under Award Numbers DE-AC05-00OR22725 sub-contract 4000158507; and under JSPS KAKENHI Grant Number JP16K18336. Discussions with team members of the RF SciDAC project (Discovery through Advanced Computing Initiative: Center for Integrated Simulation of Fusion Relevant RF Actuators) are gratefully acknowledged. This research used resources of the National Energy Research Scientific Computing Center, a DOE Office of Science User Facility supported by the Office of Science of the U.S. Department of Energy under Contract No. DE-AC02-05CH11231.

Appendix A: Solution of Maxwell's equations as a generalized eigenvalue problem

Maxwell's equations for a homogeneous plasma may be written in the form

$$\mathbf{n}\times\mathbf{B}c = -\overline{\overline{\varepsilon}}\cdot\mathbf{E} \tag{A1}$$

$$\mathbf{n}\times\mathbf{E} = \mathbf{B}c \tag{A2}$$

where $\mathbf{n} = \mathbf{k}c/\omega$. The goal of this Appendix is to formulate a generalized matrix eigenvalue problem for the component of $\mathbf{n}$ normal to a plate in the geometry of Fig. 1. It is assumed that the dielectric tensor $\overline{\overline{\varepsilon}}$ and the tangential components of the wavevector, $\mathbf{k}_t$, on the surface of the plate are known.

We first write out the x, y, and z components of Eqs. (A1) and (A2) in terms of n_x, n_y and n_z. We adopt the notation $\mathbf{k}_t = (k_{t1},k_z)$ where k_{t1} is the component in the x-y plane, Then using the rotational transformations

$$k_x = k_{t1}\cos\varphi - k_n \sin\varphi \tag{A3}$$

$$k_y = k_{t1}\sin\varphi + k_n \cos\varphi \tag{A4}$$

and moving all terms proportional to k_n to the right hand side, one arrives at the matrix equation

$$\begin{pmatrix} \varepsilon_{xx} & \varepsilon_{xy} & \varepsilon_{xz} & 0 & -n_z & n_{t1}\sin\varphi \\ \varepsilon_{yx} & \varepsilon_{yy} & \varepsilon_{yz} & n_z & 0 & -n_{t1}\cos\varphi \\ \varepsilon_{zx} & \varepsilon_{zy} & \varepsilon_{zz} & -n_{t1}\sin\varphi & n_{t1}\cos\varphi & 0 \\ 0 & n_z & -n_{t1}\sin\varphi & 1 & 0 & 0 \\ -n_z & 0 & n_{t1}\cos\varphi & 0 & 1 & 0 \\ n_{t1}\sin\varphi & -n_{t1}\cos\varphi & 0 & 0 & 0 & 1 \end{pmatrix} \begin{pmatrix} E_x \\ E_y \\ E_z \\ cB_x \\ cB_y \\ cB_z \end{pmatrix} =$$

$$n_n \begin{pmatrix} 0 & 0 & 0 & 0 & 0 & -\cos\varphi \\ 0 & 0 & 0 & 0 & 0 & -\sin\varphi \\ 0 & 0 & 0 & \cos\varphi & \sin\varphi & 0 \\ 0 & 0 & \cos\varphi & 0 & 0 & 0 \\ 0 & 0 & \sin\varphi & 0 & 0 & 0 \\ -\cos\varphi & -\sin\varphi & 0 & 0 & 0 & 0 \end{pmatrix} \begin{pmatrix} E_x \\ E_y \\ E_z \\ cB_x \\ cB_y \\ cB_z \end{pmatrix} \tag{A5}$$

This is a generalized eigenvalue problem for n_n. It is well known that the six scalar Maxwell equations contain redundancy: only four are independent. Thus the solution of this generalized eigenvalue problem yields two solutions for n_n that are formally infinite and may be discarded. The remaining four solutions are the desired four modes: incoming and outgoing fast and slow waves.

This generalized eigenvalue approach is an alternative to defining a dispersion matrix

$$\overline{\overline{\Delta}} = \mathbf{nn} - n^2\overline{\overline{I}} + \overline{\overline{\varepsilon}}, \tag{A6}$$

obtaining from det($\overline{\overline{\Delta}}$) = 0 a fourth order dispersion relation for n_n, finding its roots, and then obtaining the null space of $\overline{\overline{\Delta}}$ for each root, to give the polarization vectors.

For reference, the cold fluid dielectric tensor used in this paper is given by

$$\overline{\overline{\varepsilon}} = \varepsilon_\perp \overline{\overline{I}} + (\varepsilon_\parallel - \varepsilon_\perp)\mathbf{bb} + i\varepsilon_\times \mathbf{b} \times \overline{\overline{I}}, \tag{A7}$$

where $\varepsilon_\perp = 1 + \omega_{pi}^2/(\Omega_i^2 - \omega^2)$, $\varepsilon_\parallel = 1 - \omega_{pe}^2/\omega^2$ and $\varepsilon_\times = \omega_{pi}^2\omega/\Omega_i(\omega^2 - \Omega_i^2)$.

Appendix B: Details of the sheath boundary condition solution

The first step in the sheath BC solution is to write out the equations with $E^{(1)}$ and $E^{(2)}$ as source terms, and $E^{(3)}$, $E^{(4)}$, J_n and $\mathbf{k}\cdot\mathbf{B}_t$ as unknowns. This is a straightforward rearrangement of Eqs. (5) – (8). The second step in the Fourier method is to express $(z_{sh}J_n)$ in its Fourier representation,

$$(z_{sh}J_n)_k = \frac{1}{\sqrt{N}} \sum_{k'} z_{sh,k-k'} J_{n,k'} \tag{B1}$$

where we work in terms of the finite Fourier transform and its inverse defined by

$$F(y_i) = \frac{1}{\sqrt{N}} \sum_{k_y} F_k e^{ik_y y_i} \tag{B2}$$

$$F_k = \frac{1}{\sqrt{N}} \sum_{y_i} F(y_i) e^{-ik_y y_i} \tag{B3}$$

for any function F(y) on an equally spaced grid, y_i, where N is the number of grid points in the periodic domain. The resulting equation set for the mode with tangential wavevector component (k_{t1}, k_z) is

$$-i\omega\varepsilon_0 \mathbf{s}\cdot\overline{\overline{\varepsilon}}\cdot(E^{(3)}\mathbf{e}^{(3)} + E^{(4)}\mathbf{e}^{(4)}) - J_n = i\omega\varepsilon_0 \mathbf{s}\cdot\overline{\overline{\varepsilon}}\cdot(E^{(1)}\mathbf{e}^{(1)} + E^{(2)}\mathbf{e}^{(2)}) \tag{B4}$$

$$(E^{(3)}\mathbf{e}^{(3)} + E^{(4)}\mathbf{e}^{(4)})\cdot\mathbf{e}_t - ik_{t1}(z_{sh}J_n)_{k_{t1}} = -(E^{(1)}\mathbf{e}^{(1)} + E^{(2)}\mathbf{e}^{(2)})\cdot\mathbf{e}_t \tag{B5}$$

$$(E^{(3)}\mathbf{e}^{(3)} + E^{(4)}\mathbf{e}^{(4)})\cdot\mathbf{e}_z - ik_z(z_{sh}J_n)_{k_{t1}} = -(E^{(1)}\mathbf{e}^{(1)} + E^{(2)}\mathbf{e}^{(2)})\cdot\mathbf{e}_z \tag{B6}$$

$$-\frac{1}{\omega}(E^{(3)}k_n^{(3)}\mathbf{s}\cdot\mathbf{k}\times\mathbf{e}^{(3)} + E^{(4)}k_n^{(4)}\mathbf{s}\cdot\mathbf{k}\times\mathbf{e}^{(4)}) - \mathbf{k}\cdot\mathbf{B}_t = \frac{1}{\omega}(E^{(1)}k_n^{(1)}\mathbf{s}\cdot\mathbf{k}\times\mathbf{e}^{(1)} + E^{(2)}k_n^{(2)}\mathbf{s}\cdot\mathbf{k}\times\mathbf{e}^{(2)}) \tag{B7}$$

We define the abstract vector

$$\overline{H}_k = (E^{(3)}, E^{(4)}, J_n, \mathbf{k}\cdot\mathbf{B}_t) \tag{B8}$$

and a source term $\overline{S}_k$ which is the right hand side of Eqs. (B4) – (B7). Then the equation set takes the block matrix form

$$\overline{\overline{M}}_{k,k'} \cdot \overline{H}_{k'} = \overline{S}_k \tag{B9}$$

with an implicit sum on k′ where

$$\overline{\overline{M}}_{k,k'} = \delta_{k,k'}\overline{\overline{Q}}_k + \overline{\overline{P}}_{k,k'} \tag{B10}$$

$$\overline{\overline{Q}}_k = \begin{pmatrix} -i\omega\varepsilon_0\, \mathbf{s}\cdot\overline{\overline{\varepsilon}}\cdot\mathbf{e}^{(3)} & -i\omega\varepsilon_0\, \mathbf{s}\cdot\overline{\overline{\varepsilon}}\cdot\mathbf{e}^{(4)} & -1 & 0 \\ \mathbf{e}_t\cdot\mathbf{e}^{(3)} & \mathbf{e}_t\cdot\mathbf{e}^{(4)} & 0 & 0 \\ \mathbf{e}_z\cdot\mathbf{e}^{(3)} & \mathbf{e}_z\cdot\mathbf{e}^{(4)} & 0 & 0 \\ -\dfrac{k_n^{(3)}}{\omega}\mathbf{s}\cdot\mathbf{k}\times\mathbf{e}^{(3)} & -\dfrac{k_n^{(4)}}{\omega}\mathbf{s}\cdot\mathbf{k}\times\mathbf{e}^{(4)} & 0 & -1 \end{pmatrix} \tag{B11}$$

$$\overline{S}_k = \begin{pmatrix} i\omega\varepsilon_0\, \mathbf{s}\cdot\overline{\overline{\varepsilon}}\cdot(E^{(1)}\mathbf{e}^{(1)} + E^{(2)}\mathbf{e}^{(2)}) \\ -(E^{(1)}\mathbf{e}^{(1)} + E^{(2)}\mathbf{e}^{(2)})\cdot\mathbf{e}_t \\ -(E^{(1)}\mathbf{e}^{(1)} + E^{(2)}\mathbf{e}^{(2)})\cdot\mathbf{e}_z \\ \dfrac{1}{\omega}(E^{(1)}k_n^{(1)}\,\mathbf{s}\cdot\mathbf{k}\times\mathbf{e}^{(1)} + E^{(2)}k_n^{(2}\,\mathbf{s}\cdot\mathbf{k}\times\mathbf{e}^{(2)}) \end{pmatrix} \tag{B12}$$

$$\overline{\overline{P}}_{k,k'} = \frac{-i}{\sqrt{N}} z_{sh,k-k'} \begin{pmatrix} 0 & 0 & 0 & 0 \\ 0 & 0 & k_{t1} & 0 \\ 0 & 0 & k_z & 0 \\ 0 & 0 & 0 & 0 \end{pmatrix} \tag{B13}$$

This yields a matrix problem of dimension 4N where N is the number of grid-points on which the data for J_n and $\mathbf{k}\cdot\mathbf{B}_t$ are given.

References

[1] Wilson J R and Bonoli P T, 2015 *Phys. Plasmas* **22** 021801
[2] Hong R et al 2017 Plasma Phys. Control. Fusion **59** 105008
[3] Martin M J *et al* 2017 *Phys. Rev. Lett.* **119** 205002
[4] Bobkov V et al 2017 Plasma Phys. Control. Fusion **59** 014022
[5] Perkins R J et al 2017 Nucl. Materials and Energy **12** 283
[6] Jacquot J *et al* 2014 *Phys. Plasmas* **21** 061509
[7] Jacquet P *et al* 2014 *Phys. Plasmas* **21** 061510
[8] Ochoukov R et al 2014 Plasma Phys. Control. Fusion **56** 015004
[9] Qin C M et al 2013 Plasma Phys. Control. Fusion **55** 015004
[10] Wukitch S J *et al* 2013 *Phys. Plasmas* **20** 056117
[11] Corre Y *et al* 2012 *Nucl. Fusion* **52** 103010
[12] Noterdaeme J-M and Van Oost G 1993 *Plasma Phys. Control. Fusion* **35** 1481
[13] Perkins F W 1989 *Nucl. Fusion* **29** 583
[14] Myra J R *et al* 1990 *Nucl. Fusion* **30** 845
[15] Colas L *et al* 2012 *Phys. Plasmas* **19** 092505
[16] D'Ippolito D A *et al* 1993 *Phys. Fluids B* **5** 3603
[17] Bécoulet M *et al* 2002 *Phys. Plasmas* **9** 2619
[18] Colas L *et al* 2003 *Nucl. Fusion* **43** 1
[19] Myra J R and D'Ippolito D A 2015 *Phys. Plasmas* **22** 062507
[20] Kohno H and Myra J R 2017 Comput. Phys. Commun. **220** 129
[21] Smithe D N et al 2014 AIP Conference Proceedings **1580** 89
[22] Van Eester D 2013 *Plasma Phys. Control. Fusion* **55** 055001
[23] Myra J R and D'Ippolito D A 2010 *Plasma Phys. Control. Fusion* **52** 015003
[24] Kohno H *et al* 2012 *Phys. Plasmas* **19** 012508
[25] D'Ippolito D A *et al* 2013 *Plasma Phys. Control. Fusion* **55** 085001
[26] Kohno H *et al* 2013 *Phys. Plasmas* **20** 082514
[27] Colas L et al 2017 Plasma Phys. Control. Fusion **59** 025014
[28] Tierens W *et al* 2017 *Nucl. Fusion* **57** 116034
[29] Lu L et al 2018 Plasma Phys. Control. Fusion **60** 035003
[30] Zhang W *et al* 2017 *Nucl. Fusion* **57** 116048
[31] Jaeger E F *et al* 1995 *Phys. Plasmas* **2** 2597
[32] D'Ippolito D A and Myra J R 2006 *Phys. Plasmas* **13** 102508
[33] Myra J R 2017 *Phys. Plasmas* **24** 072507
[34] Myra J R and Kohno H 2017 *EPJ Web of Conf.* **157** 03037
[35] Kohno H and Myra J R 2019 *Phys. Plasmas* **26** 022507
[36] Takayama K *et al* 1960 *Phys. Rev. Lett.* **5** 238
[37] Stenzel R L 1988 *Phys. Rev. Lett.* **60** 704
[38] Myra J R and Kohno H 2019 *submitted to Phys. Plasmas*
[39] Elias M, Curreli D, Wright J, and Jenkins T 2019 private communication